

UNCLASSIFIED

AD 273 684

*Reproduced
by the*

**ARMED SERVICES TECHNICAL INFORMATION AGENCY
ARLINGTON HALL STATION
ARLINGTON 12, VIRGINIA**



UNCLASSIFIED

NOTICE: When government or other drawings, specifications or other data are used for any purpose other than in connection with a definitely related government procurement operation, the U. S. Government thereby incurs no responsibility, nor any obligation whatsoever; and the fact that the Government may have formulated, furnished, or in any way supplied the said drawings, specifications, or other data is not to be regarded by implication or otherwise as in any manner licensing the holder or any other person or corporation, or conveying any rights or permission to manufacture, use or sell any patented invention that may in any way be related thereto.

INTERFEROMETRIC OBSERVATION OF FLAME ACCELERATION IN AN EXPLOSIVE GAS

by

A. J. LADERMAN, P. A. URTIEW AND A. K. OPPENHEIM

TECHNICAL NOTE DR 12

FEBRUARY 1962

UNIVERSITY OF CALIFORNIA



Contract No. AF 49(638)-166

I.E.R. Project No. G-25315

273 684

ASTIA

273684

AS AD NO.

62-2-6

INTERFEROMETRIC OBSERVATION OF FLAME ACCELERATION
IN AN EXPLOSIVE GAS

by

A. J. Laderman, P. A. Urtiew and A. K. Oppenheim

TECHNICAL NOTE DR 12

FEBRUARY, 1962

UNIVERSITY OF CALIFORNIA, BERKELEY

Qualified requestors may obtain copies of this report from the ASTIA Document Service Center, Arlington Hall Station, Arlington 12, Virginia. Department of Defense contractors must be established for ASTIA services or have their "need to know" certified by the cognizant military agency of their project or contract.

This research was supported by the United States Air Force, through the Air Force Office of Scientific Research of the Air Research and Development Command under Contract AF 49(638)-166.

A B S T R A C T

Flash photographs of the transition from deflagration to detonation have been obtained by means of the Mach-Zehnder interferometer. Experiments were performed using stoichiometric hydrogen-oxygen mixtures in a 1.0 by 1.5 inch detonation tube with three methods of ignition: spark discharge, pilot flame, and glow coil. In all cases the ignitor was located at the closed end of the tube.

For each set of operating conditions, a series of flash interferograms were taken, one on each experiment, which were pieced together on a single time-space plane to yield a cinematographic representation of the process. The individual interferograms revealed considerable information on the shape of the flame front and on the structure of the reaction zone, while the sequence of photographs yielded an insight into the breakdown of the combustion front from a laminar to a turbulent flame.

TABLE OF CONTENTS

	<u>Page</u>
ABSTRACT	1
LIST OF SYMBOLS	iii
LIST OF FIGURES	iv
INTRODUCTION	1
APPARATUS	2
Interferometer	2
Light Source	4
1. Construction	4
2. Spectral Distribution	6
Detonation Tube	7
Ignition	8
Synchronization Circuit	8
EXPERIMENTAL PROCEDURE	10
RESULTS	11
Spark Ignition	11
Pilot Flame Ignition	13
Glow Coil Ignition	14
Analysis	15
1. Superposition Method	15
2. Fringe Displacement Method	17
DISCUSSION	19
SUMMARY	22
REFERENCES	24
APPENDIX	

LIST OF SYMBOLS

A_1	-	coefficient of Cauchy dispersion formula
B_1	-	coefficient of Cauchy dispersion formula
C	=	$\frac{\lambda}{KL}$
D	-	local diameter of the flame front
d	-	fringe spacing
K	=	$\frac{n-1}{\rho}$ Gladstone-Dale constant
L	-	width of the test section
l	-	distance of fringeshift from reference condition
M	-	Mach number
m	-	mole fraction
n	-	index of refraction
P	-	pressure
S	-	fringeshift
t	-	time
X_i	-	arbitrary fluid property
x	-	distance from the ignitor

GREEK SYMBOLS

γ	-	specific heat ratio
λ	-	wave length
ρ	-	density

SUBSCRIPTS

o	-	denotes undisturbed state
1	-	denotes state behind shock wave

LIST OF FIGURES

- Fig. 1 Schematic of Interferometer
- Fig. 2 Installation of Mach Zehnder Interferometer
- Fig. 3 Barium Titanate Light Source
- Fig. 4 Light Source Construction Details
- Fig. 5 Power Supply for Light Source
- Fig. 6 Spectral Transmission Curve for Filter
- Fig. 7 Power Supply for Time Delay Unit
- Fig. 8 Time Delay Unit
- Fig. 9 Delay Unit Thyatron Circuits
- Fig. 10 Block Diagram of Synchronization Circuit for Spark and Pilot Flame Ignition
- Fig. 11 Block Diagram of Synchronization Circuit for Glow Coil Ignition
- Fig. 12 Cinematographic Representation of the Development of Detonation Initial Stages with Spark Plug Ignition
- Fig. 13 Cinematographic Representation of the Development of Detonation Final Stages with Spark Plug Ignition
- Fig. 14 Cinematographic Representation of the Development of Detonation with Pilot Flame Ignition
- Fig. 15 Cinematographic Representation of the Development of Detonation with Glow Coil Ignition
- Fig. 16 Composite Interferogram - Isopycnals
- Fig. 17 P-X Profile for Fig. 16
- Fig. 18 Frame 6, Fig. 15
- Fig. 19 P-X Profile for Fig. 18

INTRODUCTION

The principal tool for the experimental investigation of the development of detonation has been high-speed photography, based on the use of either flame self-light or the schlieren method. Of these, streak techniques, where the process in the detonation tube is viewed through only a narrow slit along the tube axis, yield a representation of the space-time history of the process, while insight into the two-dimensional structure of the flow pattern has been obtained from framing photography, where a sequence of exposures of the entire cross-section of the tube is obtained. Although such records gave significant qualitative information on the transition from deflagration to detonation, neither method provided sufficient means for a quantitative determination of the thermodynamic state of the medium. Interferometry, on the other hand, has the advantage over these methods by yielding essentially a quantitative measurement of the density distribution in the flow field. The basic disadvantage results only from the limited field of view imposed by the cost of the expensive precision optical components required for interferometric observation.

The theory and operation of the interferometer as well as a summary of the various studies performed with this instrument have been described in several comprehensive publications.^(1,2) Although the Mach-Zehnder interferometer, the type most commonly used for gas-flow observation, was originally developed in the 1890's, use of the instrument was relatively limited until its revival in Germany in the late 1930's. Since then the application of the interferometer for the study of supersonic aerodynamics has been widespread. This technique was extended to the investigation of shock tube phenomena by

Mathews(3), Smith(4), and Alpher and White(5), while White(6) recently succeeded in taking interferometer still photographs of the waves which occur during the advanced stages in the development of detonation and of the fully developed detonation fronts demonstrating especially its turbulent character.

In the investigation reported here, the interferometer has been used to explore the various stages of the transition from deflagration to detonation, with a particular emphasis on the early stages of the process, that is the initial flame acceleration following ignition. For this purpose a single shot flash light source was used. The history of the process was then reconstructed by a sequence of records taken from subsequent stages in different experiments for each. Experiments were performed in stoichiometric mixtures of hydrogen and oxygen. The interferograms revealed a considerable amount of information on the structure of the reaction zone and on the breakdown from laminar to turbulent flame.

APPARATUS

Interferometer

The 8 inch Mach-Zehnder interferometer used in this investigation was designed by R. Drake, Jr., at the University of California and was patterned after the first large instrument built in this country by Eekert, Drake and Soehngen(7) for the Air Force Material Command at Wright Field, Dayton, Ohio. Details of design as well as results of experiments performed using this instrument can be found in references 8 and 9.

The instrument is shown schematically in Fig. 1. The light source (1) is focused by means of condensing lens (2) on a small plane mirror(3), which

is located at the focal point of the spherical mirror (4). The area of the mirror (3) is 2 mm sq. and it acts as the effective light source for the system. Parallel light from (4) is directed toward the beam splitter (5) where half the light is transmitted, the other half reflected toward the plane mirror (5), where it is in turn reflected through the test section to the second beam splitter (8). The reference light beam passes through the compensator plates (14) and (15) to the plane mirror (7) where it is then reflected to the beam splitter (8), combining with the light beam through the test section. Adjustment of components (7) and (8) locates the fringes in the plane of the test section, the fringes being focused on the film plane (12) by the spherical mirror (10). Between the mirror (10) and the film plane a filter (11) was installed. The compensator plates (14) are mounted in the form of a wedge and by varying the opening of the wedge the optical-path lengths of the two light beams can be made equal. Adjustment of the interferometer is made using a steady light source (17) which is focused on the electrodes of the test light source by the lens (18). All optical components, including the light source and camera are mounted on a rigid metal frame and extraneous illumination is eliminated by completely enclosing the light paths within a metal shield. Total weight of the instrument was approximately 1500 lbs.

The detonation tube, forty inches long, was installed in a vertical position. Since the interferometer field was only 8 inches, it was necessary to mount the interferometer in such a manner that it could traverse the entire length of the detonation tube. This was done, Fig. 2, by suspending the interferometer with a pulley and cable arrangement, and raising and lowering the instrument by means of a bomb loading winch. When in use the interferometer was lowered onto the Schlieren pedestals (described in reference 10) which were adjusted to the desired height. In this way, relative motion between interferometer and detonation

Light Source

1. Construction.

The light source, Fig. 3, used for these experiments was a barium titanate coaxial transmission line similar to that developed by Fitzpatrick, Hubbard and Thaler⁽¹¹⁾. Construction details are shown in Fig. 4. The barium titanate element has a hollow cylindrical shape, 2.00 inches O.D., 1.00 inch I.D., by 6 inches long. Ideally, this geometry should produce a light pulse of 0.2 μ sec duration.

A solid brass rod, which acted as the anode, was inserted in the element which, in turn, was mounted within a cylindrical brass shell, good electrical contact being insured by a silver coating deposited on the surfaces of the element. Both the rod and shell were connected to brass cones which served as electrodes. The cones, separated by a gap of 8 mm, were mounted coaxially, with their vertices facing each other. A 2 mm hole was drilled through the cones, along a common axis. In this manner the light source could be used as a point light source when it is oriented so that the discharge occurs in the direction of the optical axis, or as a line source when it is aligned with the discharge path normal to the optical axis. To minimize erosion of the cones, tungsten tips were used.

The barium titanate element, with a capacitance of 0.025 mfd was charged to 10 KV, providing a stored energy of 1.2 watt-seconds. The discharge was started by raising momentarily the potential of a third electrode, placed between the cones, to 15KV. Triggering signal was supplied by a synchronization unit described later. Power supply for the light source is shown in Fig. 5.

In this investigation the gap was aligned in the direction of

optical axis, the light source being mounted on an optical bench attached to the interferometer frame. An incandescent lamp, 17, (see Fig. 1) was used for adjustment of both the barium titanate light source, as well as the interference fringes. In spite of its large source area, the intensity of the lamp was sufficiently large to provide adequate illumination at the viewing screen. Light from the lamp was focused by the lens (18) on the aperture in the electrodes of the barium titanate light source and by the lens (2) on the small mirror (3). To insure uniform illumination over the entire test section, light emitted from the light source aperture must completely cover the mirror (3). Since the aperture and the mirror were of approximately the same size, provisions for fine adjustment (by means of micrometer screws) in three orthogonal directions were incorporated in the light source mount.

The light source was positioned by viewing it from the rear side of the mirror (3) through a translucent material (usually an exposed negative) placed between the mirror and the observer. When the mirror intercepted the light beam, a shadow of the mirror was observed on the negative. The light source was adjusted until the shadow was completely surrounded by the image of the light emitted from the aperture. Final adjustment was made to eliminate any displacement between the shadow of the mirror and the image of the light source, which could be observed as the negative was moved in the direction of the optical axis. This procedure was then repeated using the light beam from the barium titanate light source itself.

An additional factor which caused non-uniform illumination of the mirror, arose from a tendency of the discharge path to "wander", so that the discharge path was not identical on subsequent shots. This problem was reduced by confining the arc within a 2 mm I.D. soapstone tube installed

between the electrodes, at the cost of an increase in the duration of the light pulse caused by the confinement. As determined from observations with a photomultiplier tube, the light pulse duration, measured at $1/2$ peak, was 1.0 μsec and 1.5 μsec for the unconfined and confined arcs, respectively. Assuming that the maximum velocity of the waves under observation was 10^3 m/sec, then during an exposure time of 1.5 μsec , the maximum image movement at the film plane was 0.9 mm. The smear produced by an image motion of this amount is barely perceptible by eye, and, in fact, most of the photographs were quite well defined. Only in the case of glow coil ignition, where flame velocities at a position 50 cm from the ignitor (the limit of the region observed in this investigation) exceeded 10^3 m/sec, was a slight smearing of the image evident.

2. Spectral Distribution

Spectral distribution of radiant energy emitted by the discharge of the barium titanate light source was determined, using a Bausch and Lomb 33-84-25 medium size quartz spectrograph. The spectrum was recorded on Royal X Pan film, which is sensitive in the range from 2150 to 6500 Angstroms. A line spectrum was observed throughout the entire range of film sensitivity. In addition, a relatively bright continuous emission spectrum was also recorded. The strongest lines, summarized in Table I below, occurred in the visible region from 4640 to 5880 Angstroms. Relative line intensities,

TABLE I

DOMINANT LINES IN SPECTRUM OF BARIUM TITANATE LIGHT SOURCE DISCHARGE

Wave Length \AA	4640	4790	5050	5180	5510	5670	5880	
Intensity Index	3	3	1	2	4	1	2	

referred to the film exposure-density characteristic, are qualitatively indicated in the bottom row, smaller intensity corresponding to larger value of index.

The spectral range of transmission of the Borosilicate Crown Glass windows used in the detonation tube, also determined by means of the Bausch and Lomb spectrograph, was found to extend from 3250 Angstroms to well into the infrared. These limits are in good agreement with published data for similar material tabulated in reference 12. The usable light spectrum is then limited to the region between 3250 to 6500 Angstroms.

The spectral transmission curve for the filter used in this preliminary investigation is shown in Fig. 6. Although the curve extends into the infrared, this portion of the spectrum is unusable since the film emulsion cuts off at 6500 Angstroms. It was found that exposure of the film required an intensity of illumination corresponding to 20 percent transmittance. Hence, the effective band pass of the filter ranged from 5400 to 5700 Angstroms and from 6000 to 6500 Angstroms.

Detonation Tube

Experiments were performed in our $1 \times 1\frac{1}{2}$ inch detonation tube, fitted on two opposite sides with viewing windows extending, with the exception of a 2 inch section at the center, the full length of the tube. Details of the tube and gas handling system are described in reference 10. In the present case, the following modifications were made. First, to avoid condensation of water on the windows, provisions for purging the tube with hot nitrogen were added. Secondly, the top of the test section was closed by a hinged plate which was opened by the force of the explosion permitting the combustion products to escape. During the purging and filling processes, the plate was in the closed position, and the gases exhausted outside the building through rubber tubing attached to the plate.

Ignition

Three methods of ignition were used: spark discharge, pilot flame ignition, and glow coil. For all experiments the ignitor was located at the closed end of the tube. Details of the ignitors are given in reference 10; however, pertinent specifications are presented below.

For spark ignition, the electrodes, spaced $3/4$ mm apart and machined flush with the walls of the tube, were connected to the secondary of a 75:1 stepup transformer. Electrical breakdown across the gap occurred when a 0.25 μ fd capacitor at 300 V, was discharged through the primary of the transformer.

For pilot flame ignition, a small combustion chamber of approximately 7 cc volume was installed in place of the spark plug. The chamber was connected to the detonation tube by a $3/4$ mm diameter hole, 2 mm long. The mixture in the small chamber was spark ignited, and the flame propagating through the connecting orifice ignited the test gas.

The glow coil ignitor was identical in construction to the spark plug, with the exception that a small diameter coiled wire was soldered between the electrodes. The coil, of approximately one ohm resistance, was heated by energizing it with 6 VAC. In contrast to the above methods, for which ignition occurred in a matter of microseconds after the circuit was energized, the thermal capacitance of the coil caused a delay of several seconds between application of the voltage and the instant of ignition.

Synchronization Circuit

Since the interferometer field was roughly $1/3$ the size of the viewing window, synchronization of the light flash with the ignition

process was necessary in order to insure that the flame was in the field of view when the light was turned on. A special delay unit, Figs. 7,8,9, was designed for this purpose. The unit consists of two independent delay circuits, Fig. 8, which when triggered with a 10 V signal produce a 300 V output signal. For one circuit, the delay time is continuously variable from 0 to 1 msec with an accuracy of $1 \mu\text{sec}$, while for the second circuit, the delay time can be continuously varied from 0 to 3 msec with an accuracy of $3 \mu\text{sec}$. The time delay for each circuit is set by adjustment of a helipot (one for each circuit) installed on the front panel of the chassis which houses the unit. Four thyatron trigger circuits, Fig. 9, are also incorporated in the delay unit. Each circuit requires a 10 V signal to trigger the thyatron tube. Two of these circuits produce a 300 V output signal which is used for triggering other electronic equipment (e.g. oscilloscopes), the remaining thyatrons serve to drive the step-up transformers in the spark ignition and light source trigger circuits.

The block diagram of the synchronization circuit for spark and pilot flame ignition is shown in Fig. 10. The circuit was activated by introducing a trigger signal into one of the two delay units. The output of this unit (1) fired a thyatron used to drive the spark ignition transformer, and (2) triggered the second delay unit. The output of the second delay unit then fired the thyatron driving the transformer used to trigger the light source. The time delay between ignition and triggering of the light source was determined by the setting of the second delay unit, the first delay unit being used only to provide a trigger signal for the remaining circuits.

Because of the ignition delay introduced by the thermal capacitance of the coil, the above circuit could not be used with glow coil

ignition. In this instance, the light source was triggered by a signal derived from an ionization gauge, located in the vicinity of the ignitor. The block diagram for the synchronization circuit is shown in Fig. 11. When the combustion zone reached the ion gap, an electrical signal was produced, which was fed through a cathode follower, then to an amplifier which fired a thyatron, whose output was used to trigger the time delay unit. The output signal of the delay unit, in turn, triggers the thyatron used to drive the step-up transformer in the light source trigger circuit.

EXPERIMENTAL PROCEDURE

Stoichiometric hydrogen-oxygen mixtures were prepared, its composition being controlled by partial pressures of the component gases. The mixture was allowed to stand for at least several hours before use, in order to insure thorough mixing.

At the start of each day, the interferometer was brought into fine adjustment. The fringe pattern was, to a high degree, dependent on variations in room temperature, although, by continuously maintaining a constant temperature, adjustments could be reduced to a minimum and, in some cases, were unnecessary.

Several preliminary tests were first performed, using a Polaroid camera to determine the required range of time delays corresponding to the position of the interferometer field. With this established, the Polaroid camera was replaced with the Speed Graphic Camera back, and final experiments were performed with records obtained using Kodak Royal X Pan film.

The sequence of operations was as follows. The detonation tube was purged with sufficient mixture to change the volume of gas in the tube

ten to fifteen times. The shut-off valve between the tube and mixing chamber was then closed and the mixture ignited. Since a manual shutter was used, experiments were performed in total darkness, the shutter being opened just prior to ignition and closed immediately after the explosion. The detonation tube was then flushed with hot nitrogen to prevent condensation of water on the windows of the tube and have it ready for next experiment.

Each photograph was marked by the use of a metal frame attached to the cover plate of one window provided with small triangular pointers and placed 5 cm apart. These markers can be observed in the interferograms, Figs. 12-15.

RESULTS

Interferograms of the initial stages of the development of detonation are shown in Figs. 12 and 13, for spark ignition, and Figs. 14 and 15 for pilot flame and glow coil ignition respectively. Although only a single interferogram was taken on each run, all the records for a particular method of ignition have been pieced together on one x-t diagram to yield a cinematographic representation of the process. The variation in reproducibility of records obtained from subsequent runs was sufficiently small to render this method of presentation a meaningful character of a rendition of the development of the process.

Spark Ignition

The spark electrodes, flush with the inner surface of the tube, were located at the geometric center of the backwall. Immediately following ignition, the flame grew hemispherically about the spark gap, contacting the

sides of tube at $t = 250 \mu\text{sec}$, frames 1-5, Fig. 12. The surface of the flame front remained hemispherical without evidence of fine structure until $t = 500 \mu\text{sec}$, frame 9. At $t = 350 \mu\text{sec}$ a plane discontinuity appeared near the backwall, which slowly moved toward the flame, frames 7-9. At $t = 500 \mu\text{sec}$, small bumps indicating a cell structure appeared at the flame front. They became more pronounced at later times, frames 9-16, breaking finally into distributed turbulence. Flame velocity reached a maximum at $t = 600 \mu\text{sec}$ and then decelerated until $t = 1500 \mu\text{sec}$. During this period the flame front flattened, becoming almost plane at $t = 1100 \mu\text{sec}$, frame 18, Fig. 13. The reaction zone here appeared to be several centimeters thick. The flame velocity now remained nearly uniform while the flame front took on a folded appearance.

At $t = 1500 \mu\text{sec}$, shoulders of flame appeared at the wall, frames 21 and 22, which advanced ahead of the flame at the center of the tube. With the onset of the shoulders, the flame accelerated again. In approximately $100 \mu\text{sec}$, a single pronounced shoulder developed which, at $t = 1900 \mu\text{sec}$, appeared to fill the entire width of the tube. At this time the combustion front became quite asymmetric with a shoulder advancing along one side-wall substantially ahead of the rest of the flame. The reaction zone underwent evidently a period of large amplitude fluctuation, as a result of which it became distributed in space, extending over a distance of up to 10 cm.

It is apparent from frames 24-29, which were taken from different runs, that the flame shoulder advances randomly along either side of the tube. Since the detonation tube was located in a vertical position, the asymmetry of the flame front cannot be attributed to gravity forces.

Pilot Flame Ignition

Frame 1, Fig. 14, shows an undisturbed field for the first series of interferograms taken with pilot flame ignition. Curvature of the fringes was caused by wedge in the glass. In spite of this, density changes ahead of the flame could be detected by tracing the displacement of the fringes in the subsequent frames.

Although the contrast is poor, the pilot flame can be seen in the test section in frame 2, $t = 200 \mu\text{sec}$, in the approximate form of a cylinder, 1.5 cm long and 0.5 cm in diameter. During the next few hundred milliseconds the flame expanded hemispherically at the end and cylindrically at the sides and some mean motion was observed in the positive x direction, probably as a result of the motion of the burned gases which followed the flame through the orifice in the backwall.

Although flame velocities through the entire transition process were somewhat larger with pilot flame ignition than with spark ignition, flame front configuration at corresponding stages of the process were quite similar in both cases. When the flame contacted the walls of the tube, frame 6, it was dome-shaped with a cell structure clearly discernible. The cells grew then somewhat in size, the flame front becoming blunt until at $t = 600 \mu\text{sec}$, frame 10, the flame began to slow down. In frame 9, $t = 550 \mu\text{sec}$, two bands of steep density gradients are visible, one at 17 cm and the other at 18 cm, while the flame front is at 12 cm from the bottom.

At $t = 850 \mu\text{sec}$, frame 14, the flame front flattened out, but combustion zone became quite thick with a cell structure clearly evident throughout its extent. At the same time, the flame entered a new period of acceleration. At $t = 950 \mu\text{sec}$, several shoulders developed at the

walls rendering the flame front the characteristic, tulip shape, frame 16. The remaining frames show the subsequent growth of the shoulders of flame and the extension of the reaction zone as the flame front becomes still more irregular in shape.

Glow Coil Ignition

Flame velocities were much larger with glow coil ignition than with the other methods of ignition. In this case, the light source was triggered by a signal from an ionization gauge located at $x = 2.62$ cm. Frame 1, Fig. 15, was recorded at the instant when the flame front contacted the gauge. It appeared then that, during the initial stages of acceleration, the tip of the flame was about 5 cm in advance of the point where the flame touched the walls of the tube. The flame maintained its slender pointed shape for approximately 250μ sec, after which it flattened out and acquired a cell-like structure.

On frames 5, 6, 7 and 9, a shock wave can be observed several centimeters ahead of the flame, the separation increasing slightly with time. In frame 7, the shock wave is followed by a strong compression wave, as evidenced by the displacement and slope of the fringes.

Of particular interest is the appearance of a displacement of the fringes in the direction of decreasing density, immediately ahead of the flame, frame 6, whose enlargement is presented in Fig. 18. The sharp change in the slope of the fringes gives the appearance of a wave front with the same shape as the flame. While this phenomenon does not appear in frame 7, 8, 9 and 10, evidence of it does occur in frames 1-4. Here the fringes immediately ahead of the flame front also undergo a change in direction, from higher to lower density, although the zone of rarefaction is not as sharply defined as in frame 6. The only rational explanation

of this observation that might be advanced at present, is based on the consideration of the three-dimensional effects of a dome-shaped, laminar flame front with an appreciably thick preparation zone. The light refracts at first as a result of its passage across the portion of the flame in the middle of the tube giving the appearance of the first front, while the main record of the flame corresponds to the portion that extends through the whole width of the tube.

Analysis

Typical interferograms obtained with spark ignition and glow coil ignition were analyzed. In the former case, the flow ahead of the flame was continuous for the first few hundred microseconds following ignition, while in the latter case a shock wave ahead of the flame was observed almost immediately after ignition. Hence, different computation procedures were required for the determination of the state of the disturbed medium ahead of the flame in the two cases.

1. Superposition Method

With spark ignition, no evidence of a discontinuity in the flow preceding the flame was observed during the early stages of the process. The displacement of the fringes could then be followed throughout the entire flow field and the superposition method was used for the evaluation of local density distribution. The fringe pattern for the reference field was provided by an interferogram of the undisturbed test mixture taken prior to ignition. The isopycnals, that is contours of constant density, were then obtained by superimposing the no-flow fringe pattern upon its corresponding flow picture. Those regions where fringes were just 180° out of phase became visible as gray stripes, representing lines of constant

fringe shift and, therefore, constant density. A typical composite interferogram, using frame 7 of Fig. 12, is shown in Fig. 16. Nine isopycnals, the first appearing 10 cm from the backwall, can be seen ahead of the flame. Other measurements have indicated that the flow preceding the flame can be considered isentropic. Hence the pressure, local speed of sound, particle velocity, etc., are uniquely determined by the density, and the isopycnals then represent also constant pressure contours, or pressure fronts. In our previous work it was found that the shape of the pressure fronts generated at the flame front, at least those of finite strength, quickly becomes planar and normal to the direction of propagation. In Fig. 17, the isopycnals, while plane, are somewhat oblique to the tube axis, the angle of inclination increasing towards the front of the pressure wave. This might be due to a slight displacement of the glass, or it may be a true indication of the fact that a continuous pressure wave, unlike the discontinuous shock, is indeed non-uniformly distributed over the tube cross-section as a result of a weaker coupling across its front.

The local density, ρ , was computed from the relationship

$$\frac{\rho}{\rho_0} = 1 + \frac{\lambda S}{(n_0 - 1)L} \quad (1)$$

where λ is the wave length of light, n_0 the corresponding index of refraction, S the fringe shift expressed as a multiple of the fringe spacing, L the width of the test section, and the subscript 0 denotes the undisturbed state. Because of the continuous emission spectrum superposed on the line spectrum of the light source, λ varied from 5400 \AA to 5700 \AA , the bandpass of the filter. However, the variation

of n_0 over this range of wave length was negligible and calculations were performed using $n_0 = 1.0001635$ corresponding to $\lambda = 5510 \text{ \AA}$.

The space profile of local density and pressure, the latter computed as an isentropic constant exponent, are plotted in Fig. 17. Included also is the pressure profile obtained from previous measurements with a pressure transducer¹⁰. The pressure evaluated from the interferogram was everywhere larger than that measured with the transducer, reaching a maximum of 30 psia at flame front where the measured pressure was only 24 psia. Although the agreement between the two curves is not particularly good, some portion of the discrepancy can be logically attributed to the non-reproducibilities in the process which occurs on subsequent shots.

2. Fringe Displacement Method

Fig. 18, obtained with glow coil ignition, shows evidence of a shock wave propagating into the undisturbed medium, followed by a continuous compression wave and, finally, by the flame. Since the shock front is too narrow to resolve, the fringe shift across the shock cannot be traced; hence the shock strength cannot be determined from the interferogram. However, from our previous Schlieren observations, the shock wave Mach number, during this same stage of the process, was found to be $M = 1.49$. The corresponding pressure and density ratios across the shock were then evaluated, using the normal shock wave relations, to serve as the reference state behind the shock. Choosing a particular fringe between the shock wave and the flame, the pressure and density in this region were then computed by the simple relation

$$\frac{P}{P_1} = \left[1 + \frac{\lambda}{(n_1 - 1)L} \left(\frac{e}{d} \right) \right]^{7\gamma} = \left(\frac{\rho}{\rho_1} \right)^{\gamma}$$

where d is the distance between dark (or light) fringes in the reference condition, ℓ the distance shifted by a dark (or light) fringe, and subscript 1 denotes the reference state immediately behind the shock. The fringe spacing, d , was easily determined from the undisturbed medium ahead of the shock and the fringe shift, ℓ , was taken as the lateral displacement (in the y direction) of the fringe from its position immediately behind the shock wave. The index of refraction, n , was evaluated using the Gladstone-Dale constant, $K = (n-1)/\rho$.

Since the wave front which defined the rarefaction zone immediately ahead of the flame was not planar, the observed fringe shift did not represent the actual density change which occur there. Assuming, as a first approximation, that the region of rarefaction was axially symmetric, the true fringe shift along the axis of symmetry (which corresponded closely to the axis of the tube) was obtained by multiplying the observed displacement of the fringe from its position at the wave front by the ratio D/L , where D is the local diameter of the rarefaction front, and L is the width of the test section. Local pressures in the region between the flame and shock wave were computed using the isentropic law with a constant exponent. Although this relation is valid through the compression wave, it may not be applicable through the rarefaction where the chemical reaction may be in progress.

The calculated density and pressure ratios are shown in Fig. 19, where, for comparison, the pressure profile obtained from previous measurement with a pressure transducer¹⁰ is included. Although the maximum pressures determined by both methods are in good agreement, the pressure-distance profiles through the compressed medium have different rates of rise. The difference, however, is sufficiently small to ascribe it to the relative non-reproducibility of the process.

DISCUSSION

It is of interest to compare our results with those obtained by other means of observation. Flame structure was observed by Salamandra et al¹³, who investigated the transition from deflagration to detonation in spark ignited stoichiometric hydrogen-oxygen mixtures initially at NTP using both streak and multiple flash Schlieren photography. The shape of the flame world line recorded by them is in good agreement with that observed in the present study and in our previous Schlieren work¹⁰. Immediately following ignition, the flame experienced an initial acceleration, followed by a period of gradual slowing down, and finally by a renewed acceleration, which eventually led to the establishment of detonation. Just before and throughout the second phase of acceleration, the flow field behind the flame front appeared quite disturbed. A similar phenomenon was observed in our own streak Schlieren photographs. While Salamandra et al do not attach any particular importance to the additional disturbances, in our opinion they are indicative of the actual structure of the reaction zone. This seems quite reasonable in view of the agreement between the width of the reaction zone observed in our flash photographs of the flame front, and the extent of the optical non-homogeneities which appear behind the flame in the streak Schlieren records¹⁰.

The development of the process was interpreted by Salamandra et al, on the basis of a series of flash Schlieren photographs taken across the full width of the observation window in order to reveal the shape of the flame front. Explaining the initial phase of flame acceleration, the authors state:

"During slow combustion, a small pressure drop in the reaction zone is accompanied by a considerable increase in the specific volume of the combustion products as compared with the specific volume of the combustible mixture prior to combustion. The expansion of the combustion product results in the appearance of a fresh gas flow before the flame front."

The gas motion ahead of the flame is then considered similar to the gas movement in front of a piston accelerating in the same manner as the flame. During this period the flame is dome shaped, in agreement with our own observations.

The argument presented by Salamandra et al to explain the deceleration period is unconvincing. They write:

"As the flame propagates and the volume of the burned mixture expands, the expansion ratio of the reaction products decreases and the flame propagates at a slower rate. Finally, there comes a moment when the pressure after the front becomes lower than the pressure before the front. This causes the formation of a new flow in the direction opposite to that of flame propagation."

Flash photographs of the flame during this stage of the process, which they point out in support of their theory, show shoulders of flame advancing along the walls of the tube ahead of the center position of the flame. This particular flame front configuration is referred to as a tulip-shaped flame.

The above statements imply the existence of an intermediate stage during which the pressure behind the reaction zone was greater than the pressure ahead of it. For an expansion ratio greater than one, such a flame is physically inadmissible, since it propagates with an imaginary velocity. This is a well known consequence of the properties of the Rayleigh Line and is pointed out by Oppenheim¹⁴ and by Troshin¹⁵ who, investigating region of deflagration during the transition to detonation, demonstrated that the pressure behind the flame is always lower than the pressure ahead of it. In fact, the pressure drop across the flame continuously increases with increased flame velocity, reaching a maximum for a C-J deflagration. Furthermore, if a flow reversal is to be associated with a pressure drop across the flame front, then a reverse flow would be expected throughout the entire transition process. Obviously, this cannot be the case.

Martin^{6,16} recorded flame front structure during the development of detonation by means of flame self-light photography. He accomplished this by photographing the flame front as it passed a slit placed normal to the axis of propagation with a rotating mirror camera. Although Martin's experiments were performed with acetylene-oxygen mixtures at low initial pressures, it is felt that the mechanism of flame acceleration is similar under all conditions and that his results may be used as basis for comparison. The flame front pattern observed by Martin resembled those recorded by Salamandra et al and, in addition, transition in the shape of the flame front occurred in the same sequence. In particular, Martin observed that, following a period during which the flame front was dome shaped, transition to a tulip-shaped flame occurred with shoulders appearing at the wall advancing ahead of the center position of the flame. However, in contrast to the observations of Salamandra et al, this occurred when the flame was accelerating, and it was attributed to the development of turbulence in the boundary layer.

Our own observations also show that the flame was initially hemispherical in form and later became tulip-shaped, but always during a period of acceleration. This configuration is clearly evidenced for pilot flame ignition, Fig. 14, and, to a lesser degree, for spark ignition, Fig. 13. The fact that the flame front should acquire this shape when accelerating is entirely reasonable, because the flame front surface area is then increased leading to the generation of pressure waves, which accelerate the unburned mixture ahead of the flame. If the development of shoulders in the flame front can indeed be attributed to turbulence, this process would magnify the turbulence, causing further increase in flame front surface area with the generation of additional pressure waves and renewed acceleration.

These three investigations, where observations were made using different optical techniques show that, during the initial stages of the development of detonation, the structure of the flame front undergoes the following changes:

- 1) immediately following ignition the flame front is dome-shaped
- 2) then shoulders of flame appear at the wall, and the flame front becomes tulip-shaped
- 3) finally the flame front breaks down completely acquiring an asymmetric form and the reaction zone increases appreciably in extent.

SUMMARY

Flash interferometric observations have been made of the transition from slow burning to detonation in stoichiometric mixtures of hydrogen and oxygen initially at NTP. Ignition was executed by means of either spark discharge, pilot flame, or glow coil, each ignitor being located at the backwall of the detonation tube. Observations were restricted to the initial stages of flame acceleration, before the establishment of detonation.

The photographs revealed considerable information on the flame front configuration and on the structure of the reaction zone. For spark discharge ignition, the following features were observed. Immediately following ignition, the flame was laminar, having the form of a smooth dome, and propagated at an accelerating rate. After several hundred μ sec, the flame experienced a slight slowing down, during which the shape of the flame became flatter and the combustion zone acquired a cell-like structure. This was followed, after

several hundred μ sec, by the development of shoulders of the flame at the wall, advancing ahead of the central portion of the combustion front. During this time flame acceleration was renewed. Eventually one shoulder became predominant, the flame front assuming an asymmetric form, and the reaction zone extending over a distance of some 10 to 15 cm.

Once the flame completely filled the tube cross section, the results with pilot flame ignition were quite similar to those obtained with ignition by spark discharge. However, with glow coil ignition, the breakdown to a turbulent flame was not observed over the region investigated.

REFERENCES

1. Ladenburg, R. and Bershader, D., Article A 3 in Physical Measurements in Gas Dynamics and Combustion, Vol IX of High Speed Aerodynamics and Jet Propulsion. Princeton University Press, Princeton, 47-78, 1954.
2. Holder, D.W., North, R.J. and Wood, G.P., Optical Methods for Examining the Flow in High Speed Wind Tunnel, AGARDograph 23, 1956.
3. Matthews, P.L., Interferometric Measurements in the Shock Tube of the Dissociation Rate of Oxygen. Physics of Fluids, 2, 17-178, 1959.
4. Smith, W.R., Mutual Reflection of Two Shock Waves of Arbitrary Strengths. Physics of Fluids, 2, 533-541, 1959.
5. Alpher, R.A. and White, D.R., Optical Refractivity of High Temperature Gases. I. Effects Resulting from Dissociation of Diatomic Gases. Physics of Fluids, 2, 153-161, 1959. II. Effects Resulting from Ionization of Monatomic Gases. Physics of Fluids, 2, 162-169, 1959.
6. Martin, F.J. and White, D.R., The Formation and Structure of Gaseous Detonation Waves. Seventh Symposium (International) on Combustion, 229-238, Butterworths Scientific Publications, London, 1959. See also, White, D.R., Turbulent Structure of Gaseous Detonation. Physics of Fluids, 4, 465-480, 1961.
7. Eckert, E.R.G., Drake, R.M. Jr., and Soehngen, E., Manufacture of a Mach-Zehnder Interferometer. Air Force Technical Report 5721, 1948.
8. Wong, G.S., Determination of Local Heat Transfer Coefficient for Free Convection for a Cylinder in Air with the Mach-Zehnder Interferometer. M.S. Thesis, University of California, Berkeley, 1950.
9. Doughty, D.L., The Application of a Mach-Zehnder Interferometer to the Study of Local Forced Convection Heat Transfer from a Cylinder. M.S. Thesis, University of California, Berkeley, 1951.
10. Laderman, A.J. and Oppenheim, A.K., Experimental Study of the Development of Detonation. Technical Note DR 9, AFOSR TN60-1303, University of California, November 1960.
11. Fitzpatrick, J.A. Hubbard, J.C., and Thaler, W.J., High Intensity Short Duration Spark Light Source. Journal of Applied Physics, 21, 1269-1271, 1950.
12. Jenkins, F.A. and White, H.E., Fundamentals of Optics, McGraw-Hill Book Co., Inc., New York, 1957.

13. Salamandra, G.D., Bazhenova, T.V. and Naboko, I.M., Formation of Detonation Wave During Combustion of Gas in Combustion Tube. Seventh Symposium (International) on Combustion, 851-855, Butterworths Scientific Publications, London, 1959. See also: The Formation of a Detonation Wave During the Combustion of Gas in Pipes. Zhurnal Tekhnicheskoi Fiziki, 29, 1354-1359 (In Russian).
14. Oppenheim, A.K., A Contribution to the Theory of the Development and Stability of Detonation in Gases, Journal of Applied Mechanics, 19, No. 1, 67-71, March 1952.
15. Troshin, Ya K., The Generalized Hugoniot Adiabatic Curve. Seventh Symposium (International) on Combustion, 789-798, Butterworths Scientific Publications, London, 1959.
16. Martin, F.J., Transition from Slow Burning to Detonation in Gaseous Explosives. Physics of Fluids, 1, 399-407, 1958.

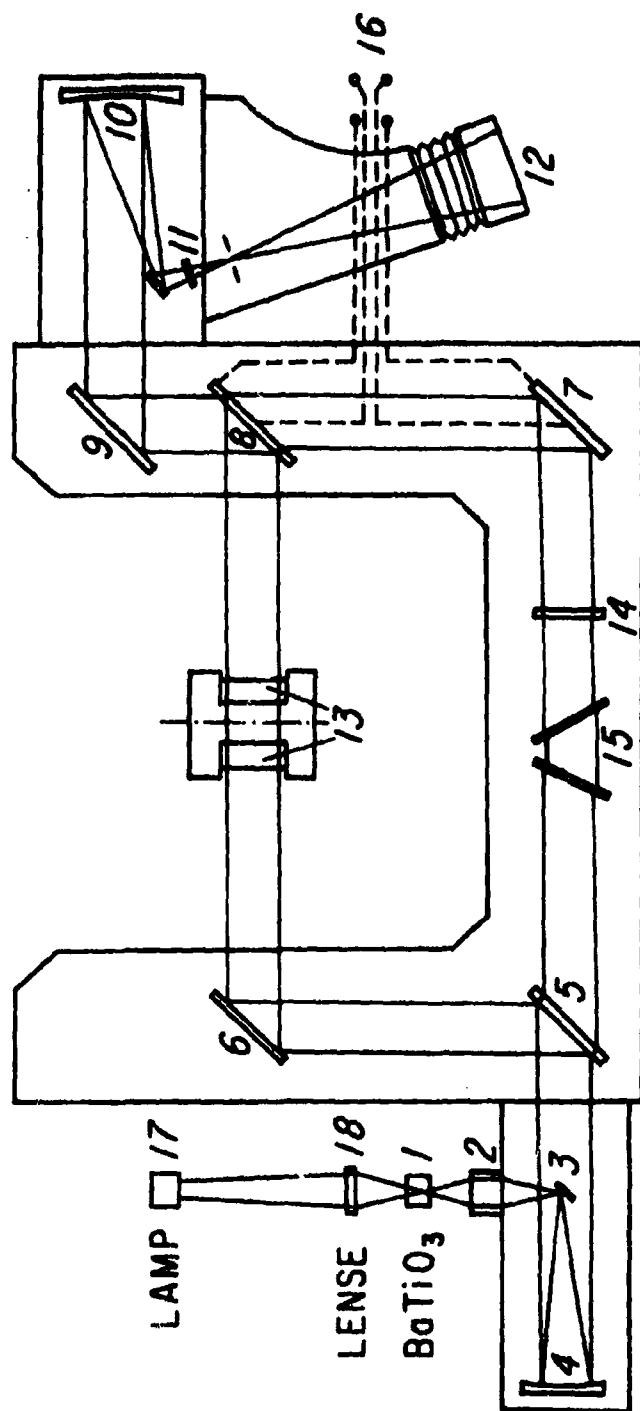


FIG. 1. SCHEMATIC OF INTERFEROMETER

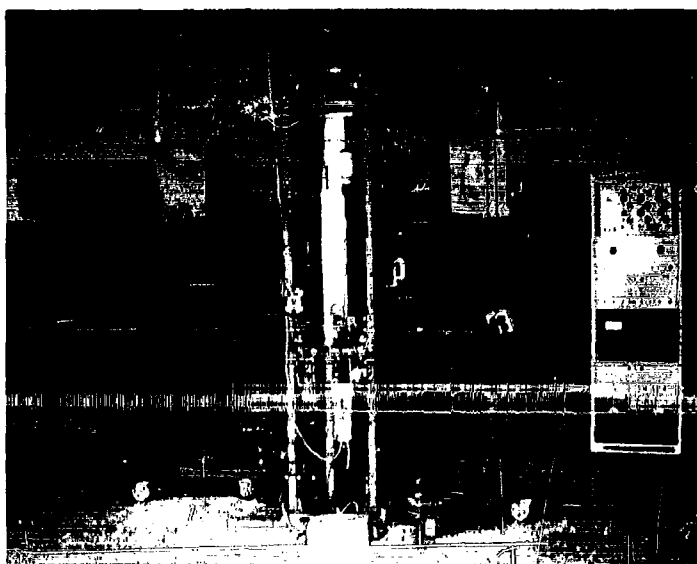


FIG. 2. INSTALLATION OF MACH ZEHNDER INTERFEROMETER

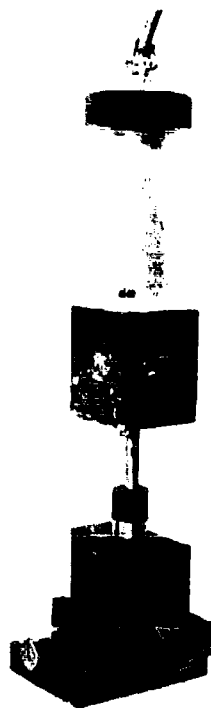


FIG. 3. BARIUM TITANATE LIGHT SOURCE

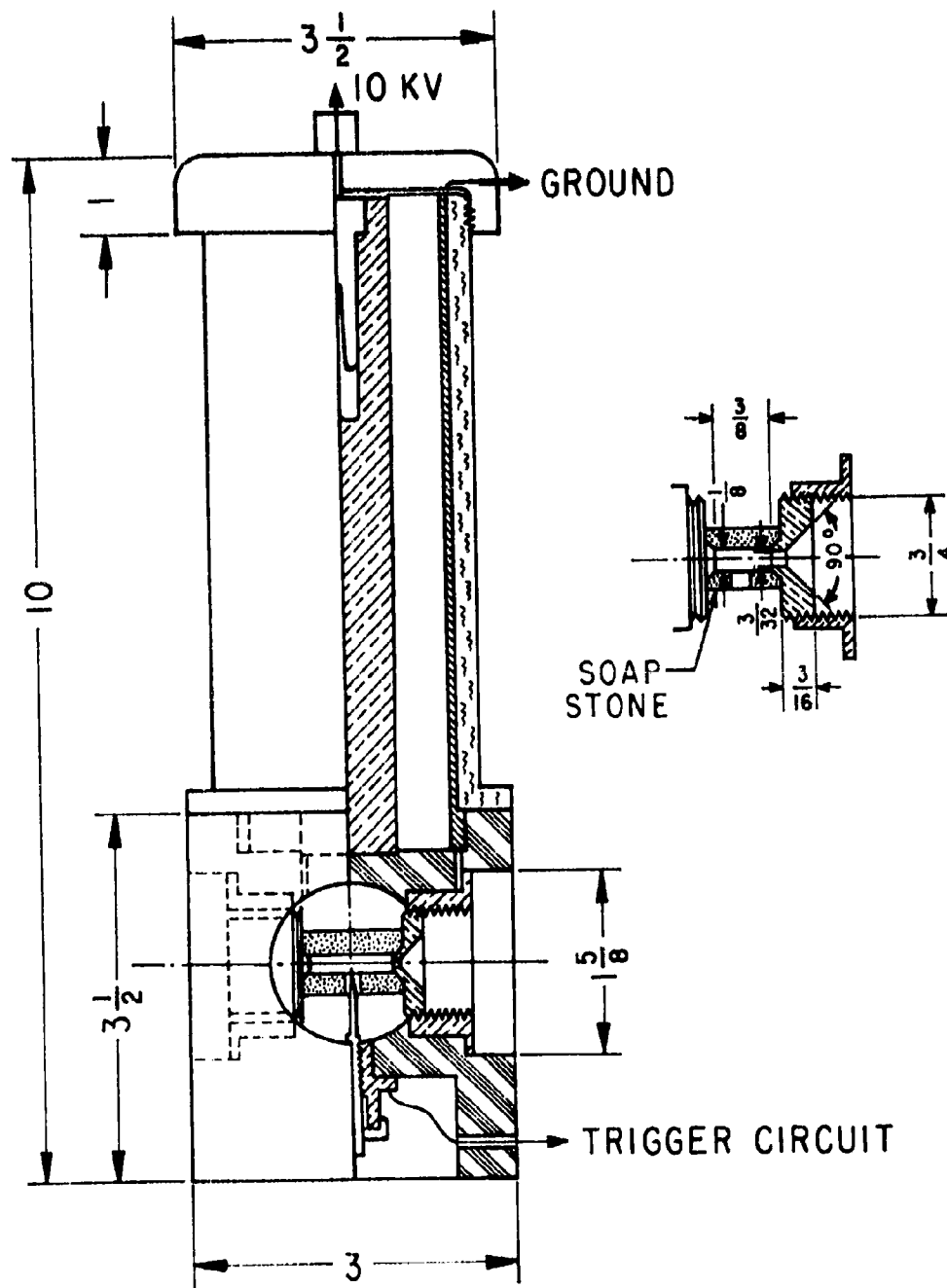


FIG. 4. LIGHT SOURCE CONSTRUCTION DETAILS

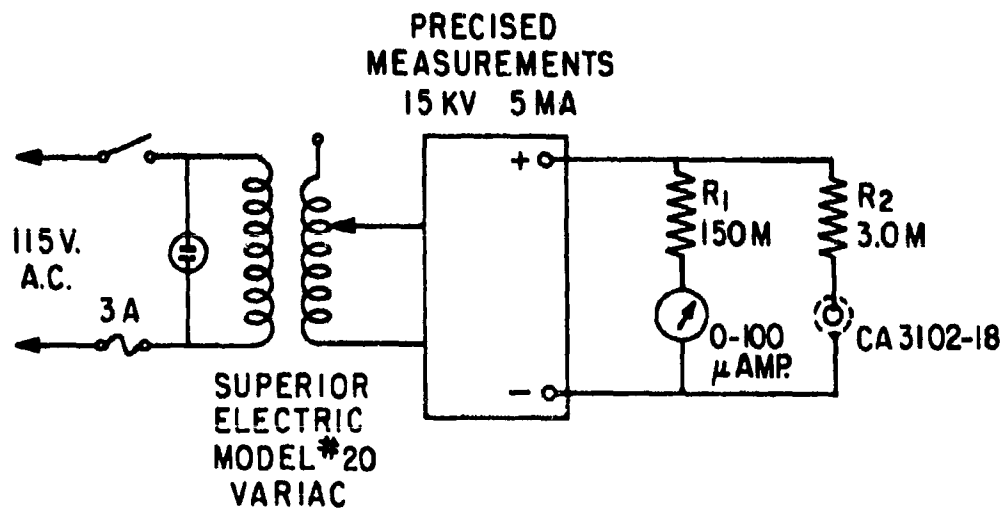


FIG. 5. POWER SUPPLY FOR LIGHT SOURCE

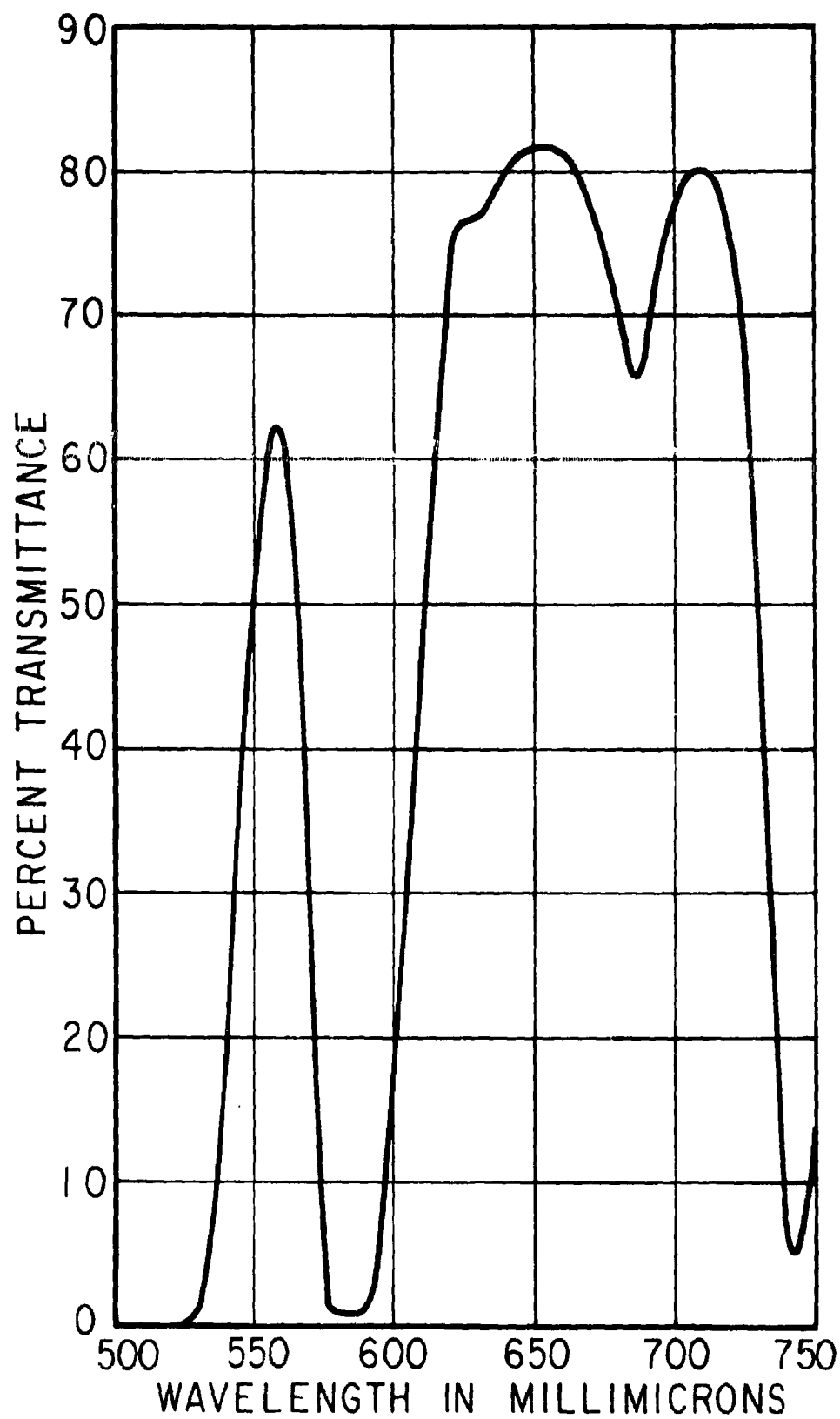


FIG. 6. SPECTRAL TRANSMISSION CURVE FOR FILTER

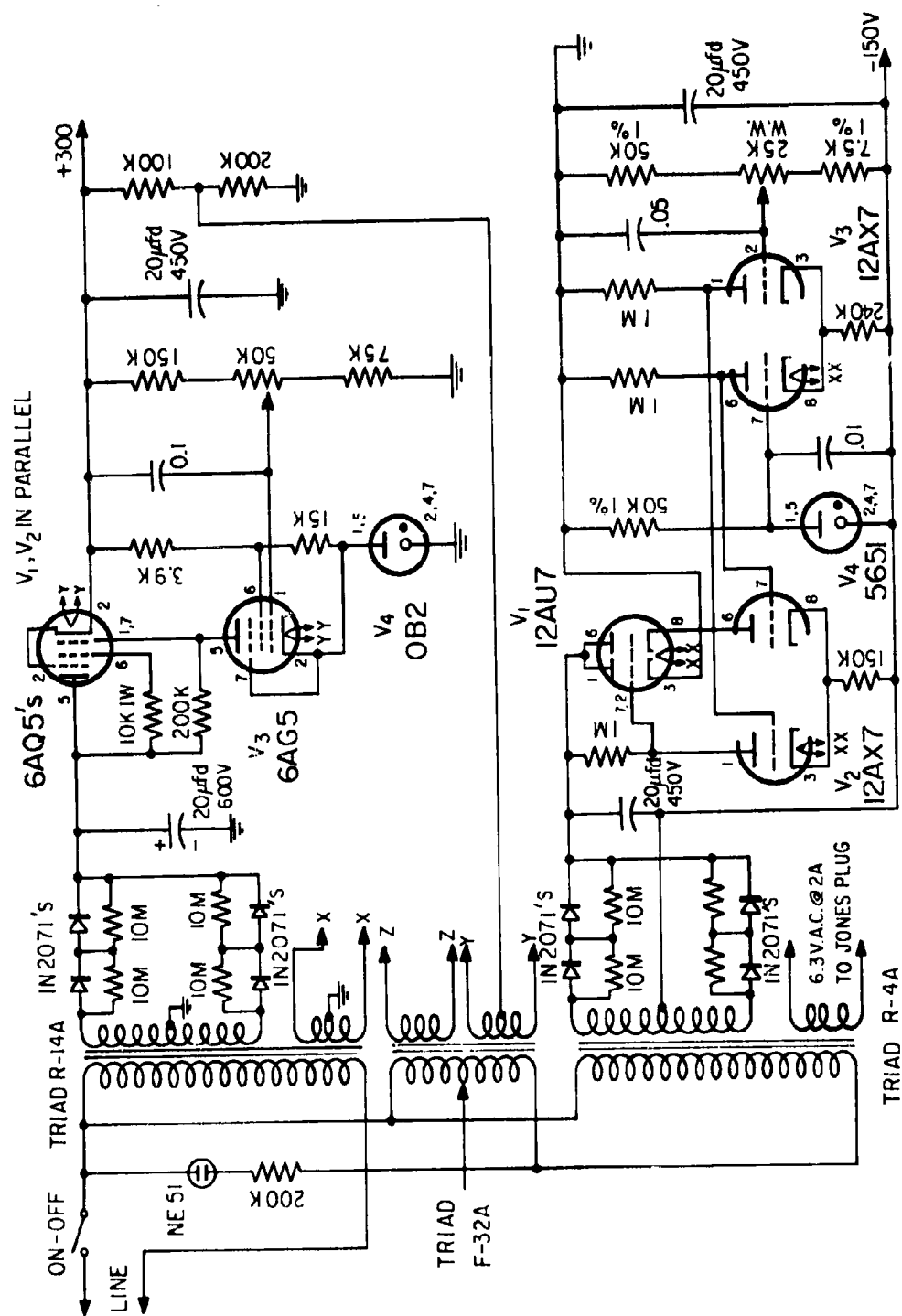
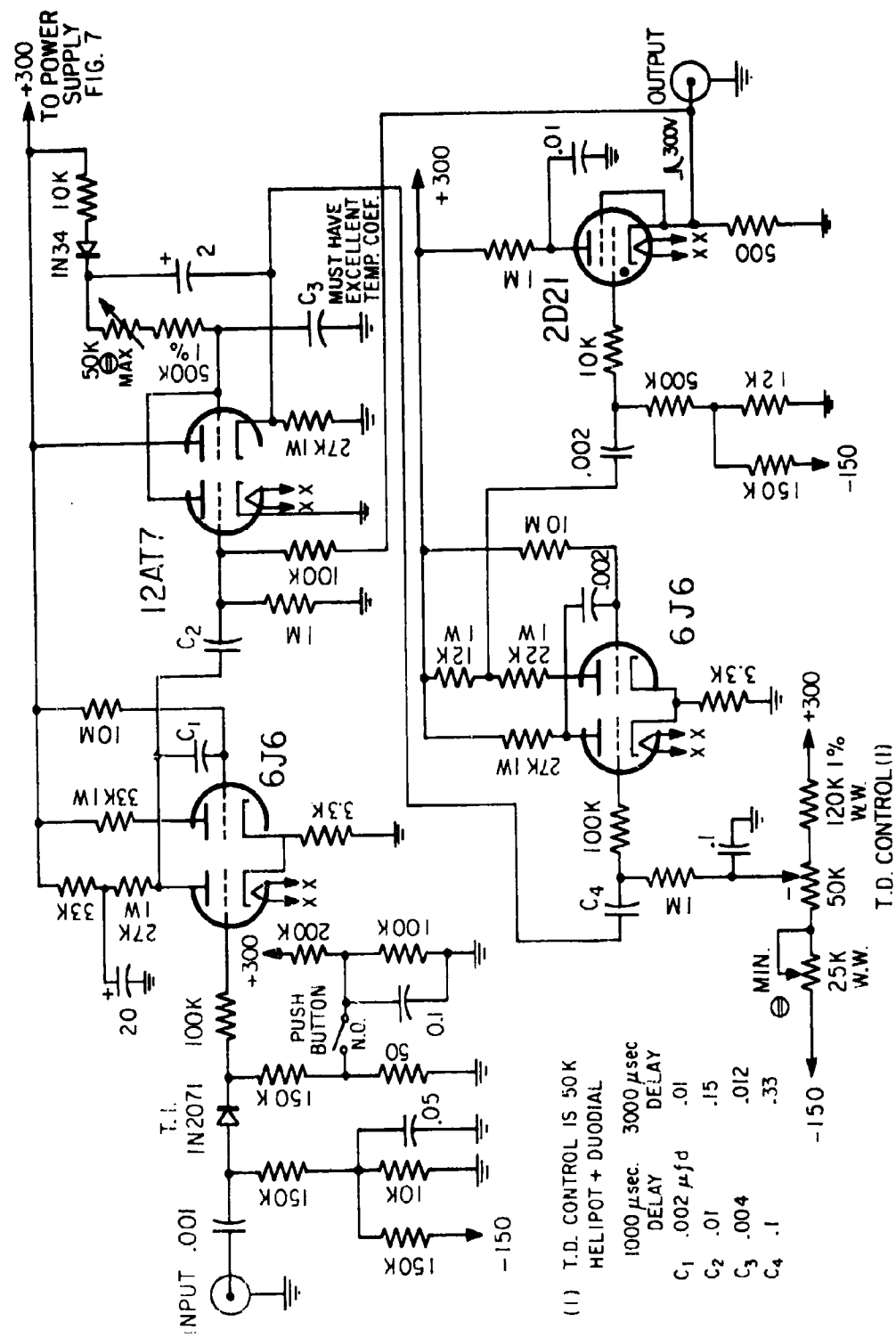


FIG. 7 POWER SUPPLY FOR TIME DELAY UNIT



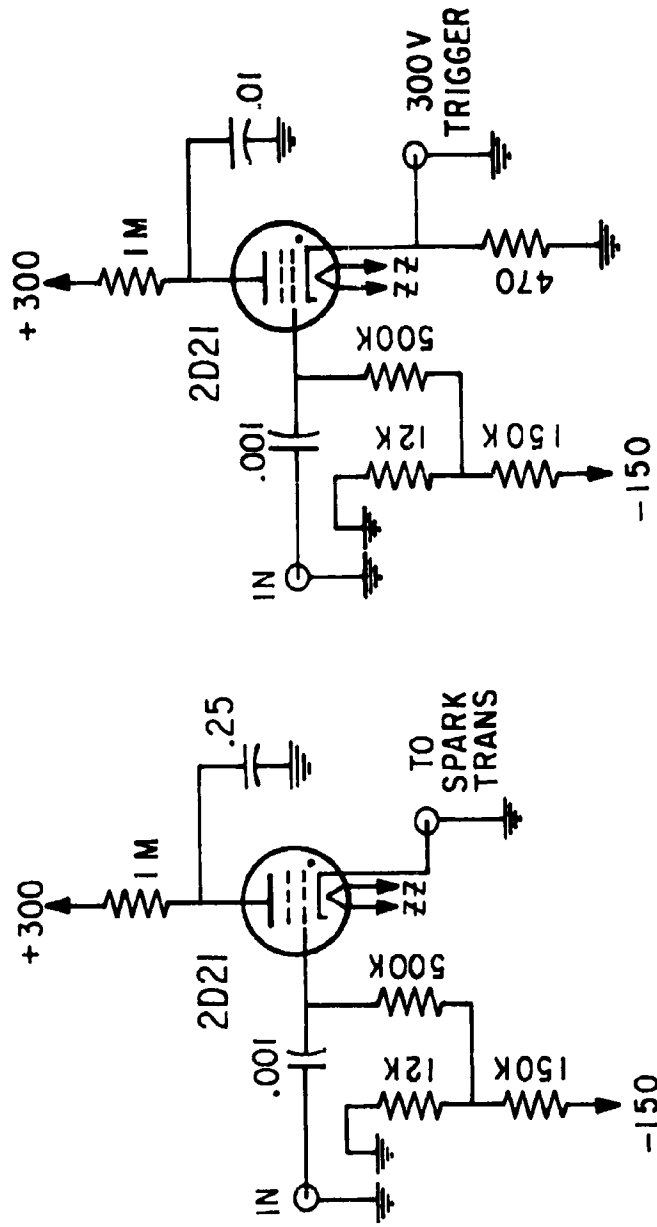


FIG. 9. DELAY UNIT THYRATRON CIRCUITS

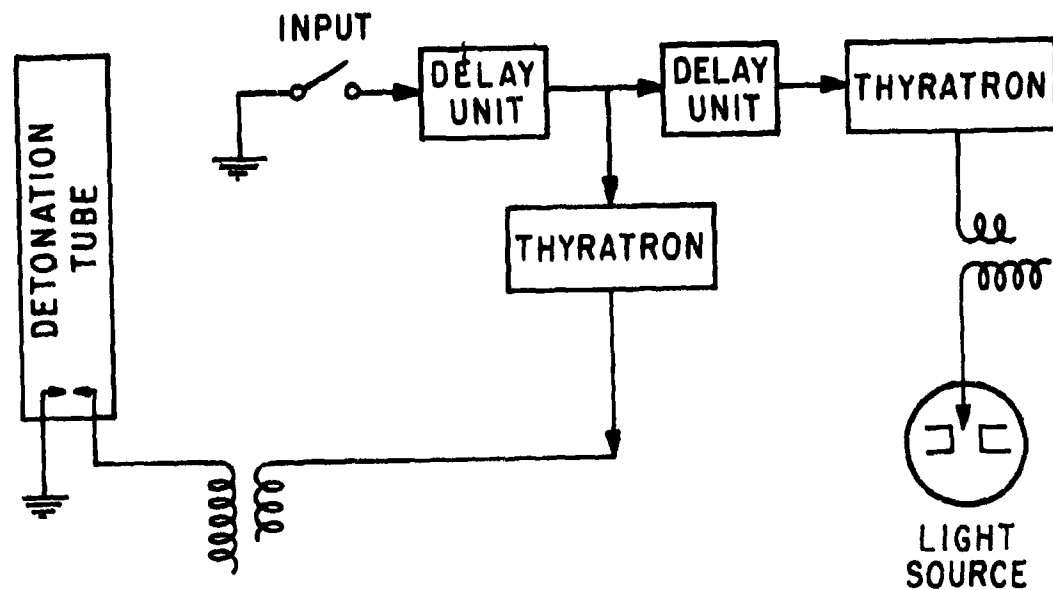


FIG. 10. BLOCK DIAGRAM OF SYNCHRONIZATION CIRCUIT FOR SPARK AND PILOT FLAME IGNITION

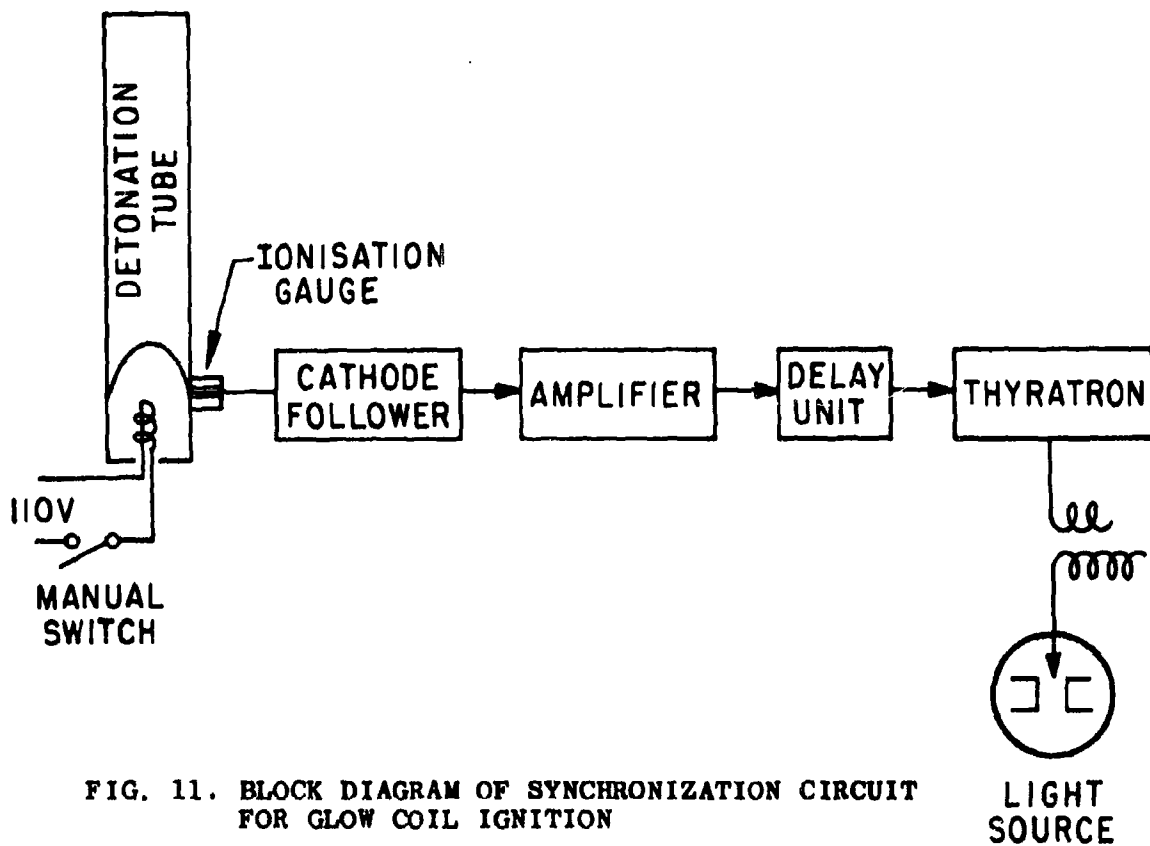


FIG. 11. BLOCK DIAGRAM OF SYNCHRONIZATION CIRCUIT FOR GLOW COIL IGNITION

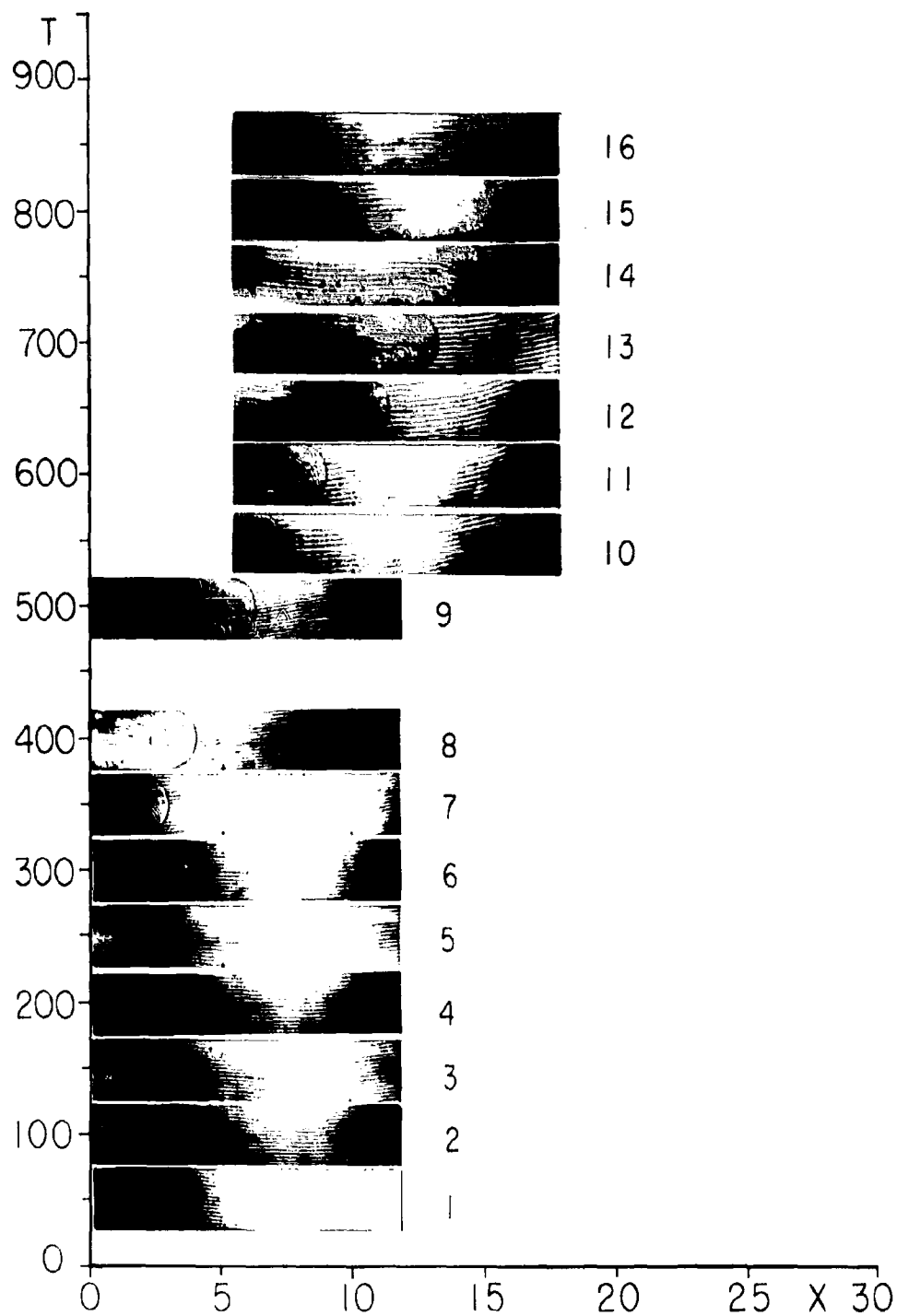


FIG. 12. CINEMATOGRAPHIC REPRESENTATION
OF THE DEVELOPMENT OF DETONATION
INITIAL STAGES WITH SPARK PLUG IGNITION

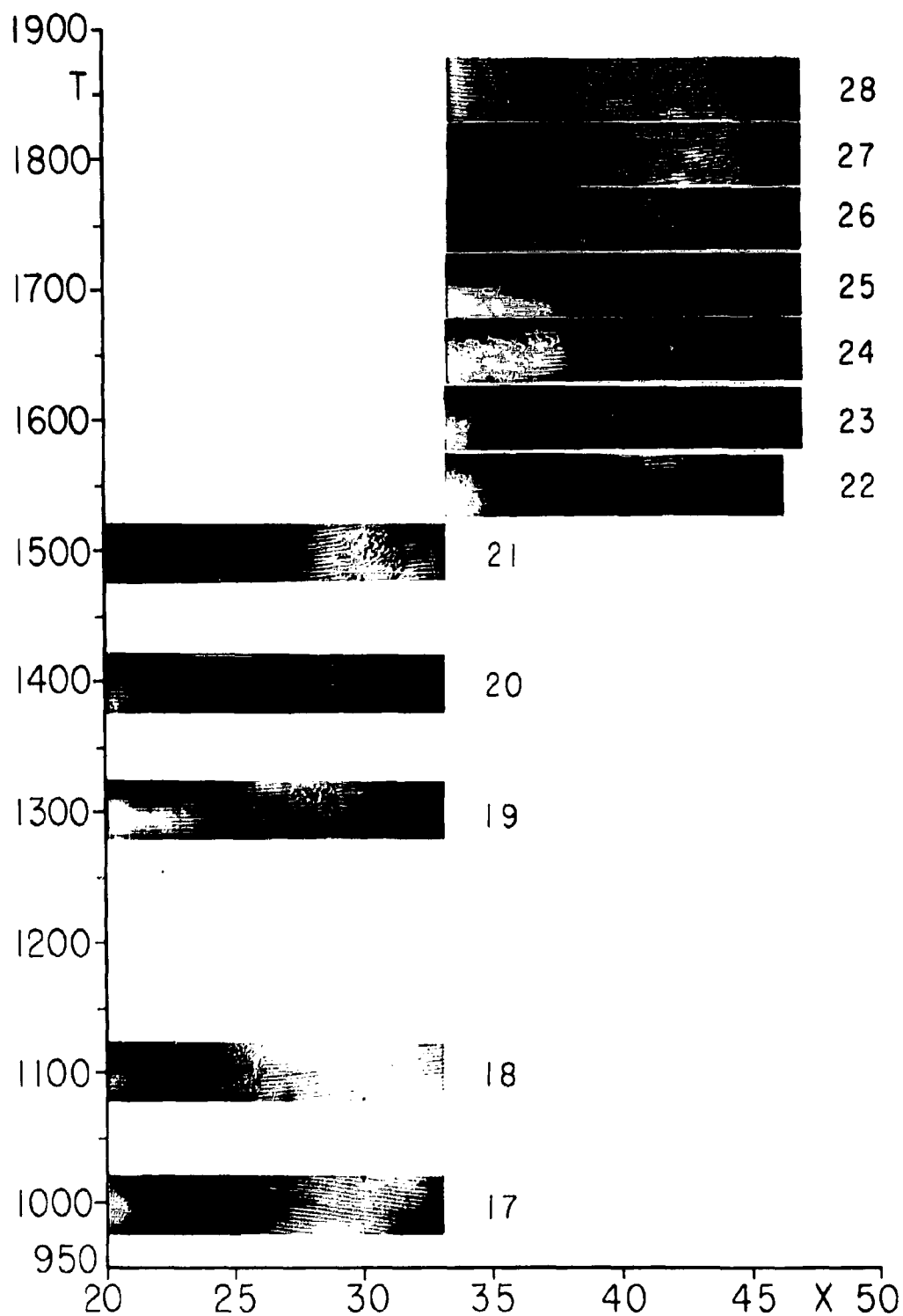


FIG. 13. CINEMATOGRAPHIC REPRESENTATION
OF THE DEVELOPMENT OF DETONATION
FINAL STAGES WITH SPARK PLUG IGNITION

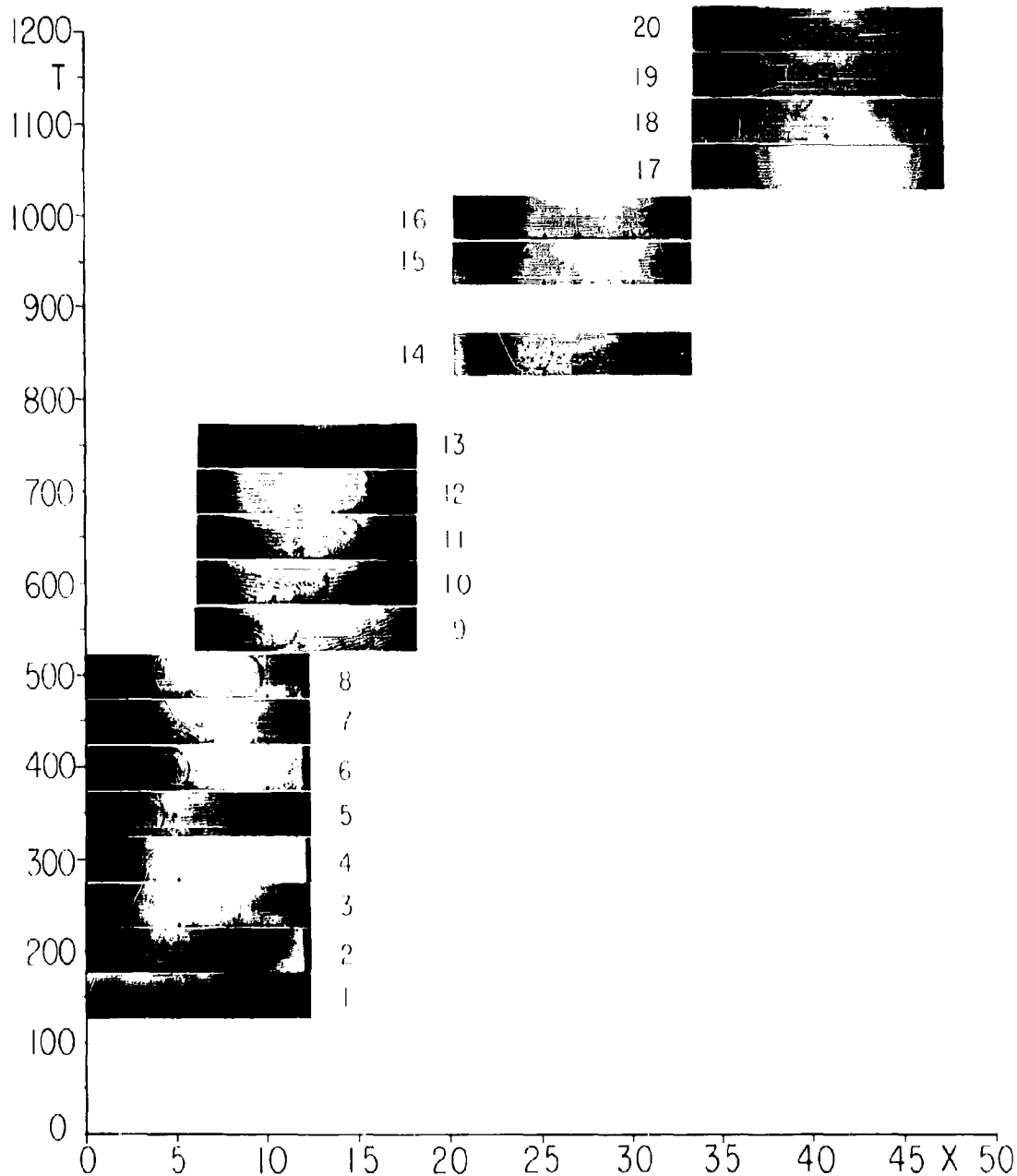


FIG. 14. CINEMATOGRAPHIC REPRESENTATION
OF THE DEVELOPMENT OF DETONATION
WITH PILOT FLAME IGNITION

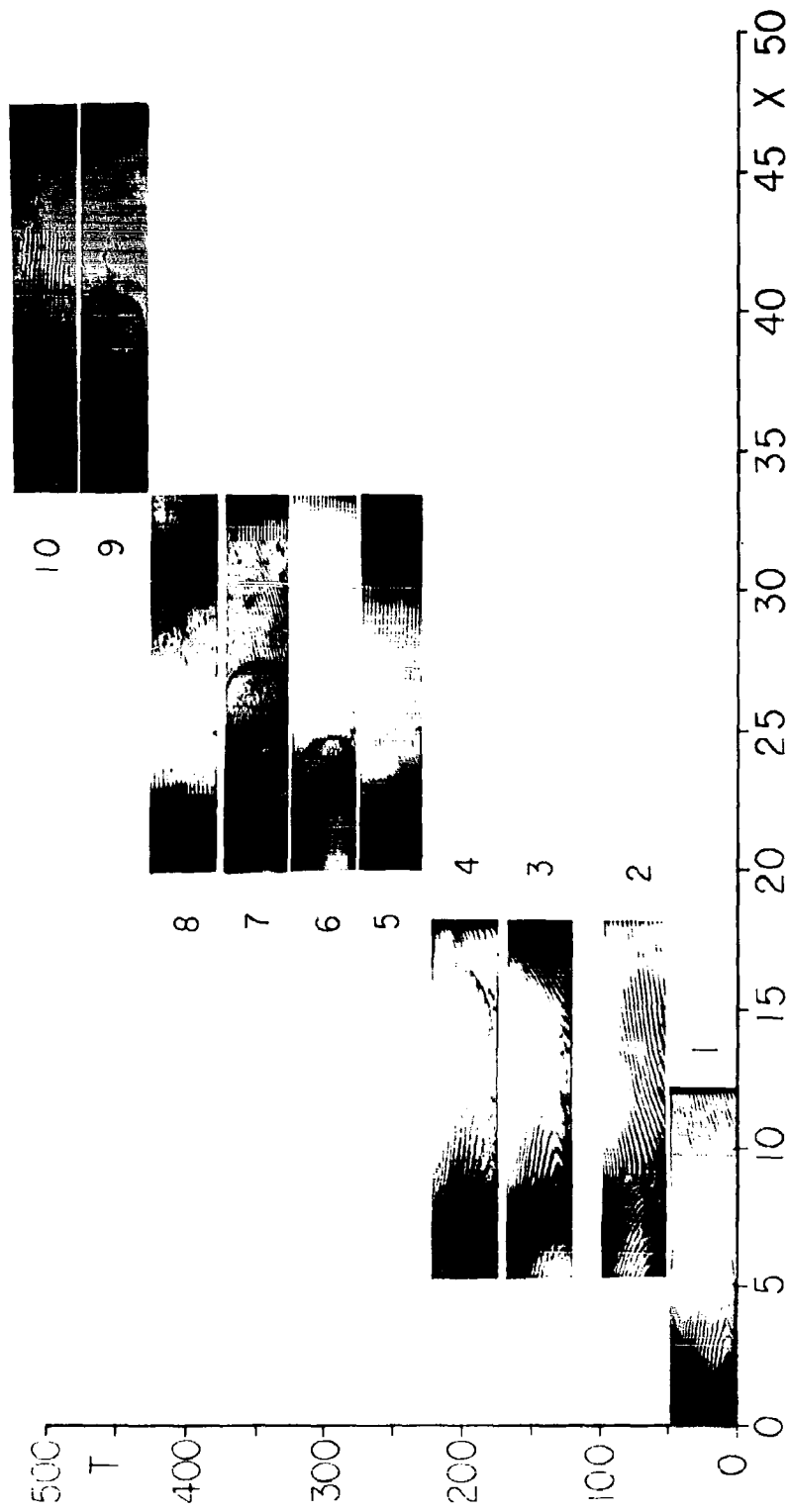


FIG. 15. CINEMATOGRAPHIC REPRESENTATION
OF THE DEVELOPMENT OF DETONATION
WITH GLOW COIL IGNITION



FIG. 16. COMPOSITE INTERFEROGRAM - ISOPYCNALS

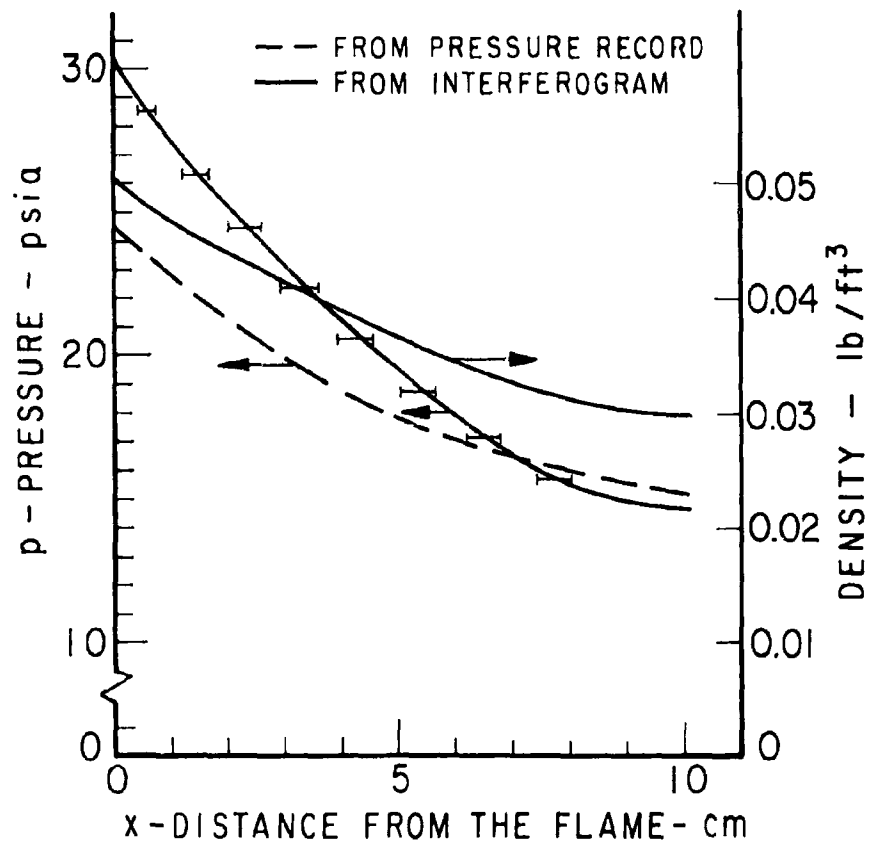


FIG. 17. P-X PROFILE FOR FIG. 16

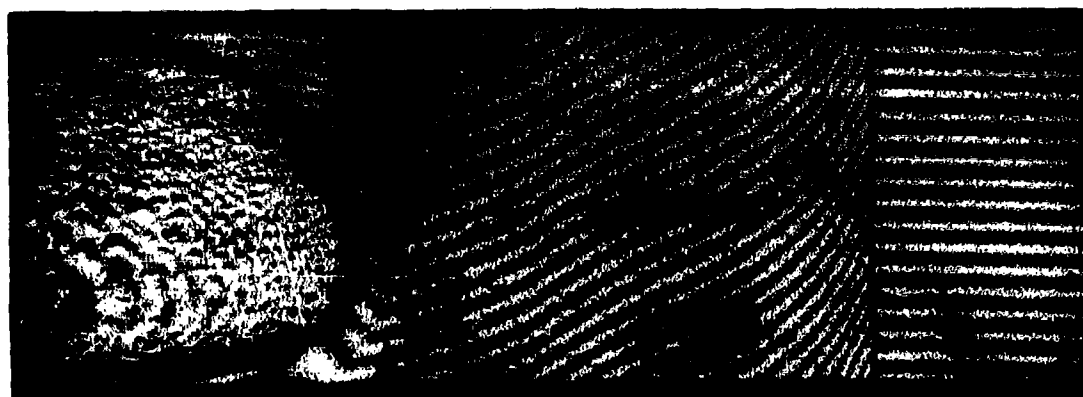


FIG. 18. FRAME 6, FIG. 15

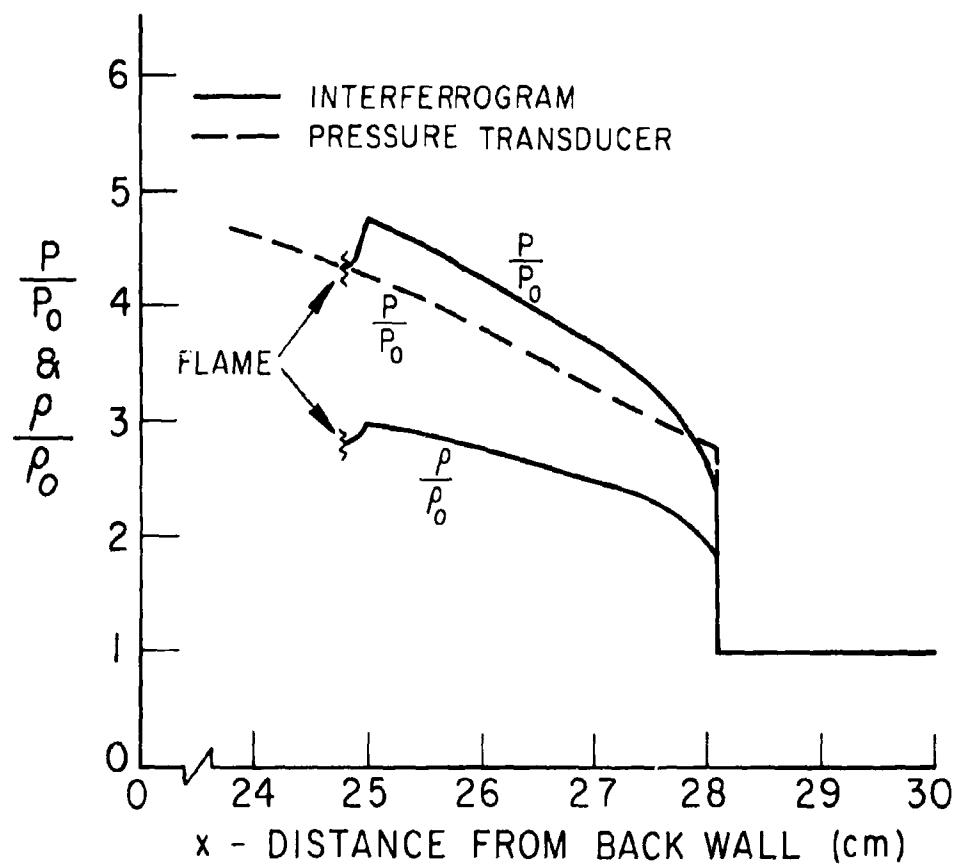


FIG. 19. P-X PROFILE FOR FIG. 18.

APPENDIX

TABLE OF CONTENTS

	<u>Page</u>
COMPUTATION OF DENSITY	A1
Superposition Method	A1
Fringe Displacement Method	A4

TABLES

A.1	Coefficients of the Cauchy Dispersion Formula	A2
A.2	Calculation of Density and Pressure in Flow Ahead of the Flame	A7
A.3	Calculation of Density and Pressure in Flow Ahead of the Flame	A8

COMPUTATION OF DENSITY

Superposition Method

Contours of constant density can be conveniently determined by superposing an interferogram of the undisturbed field with one taken during the experiment. When the fringes on the two interferograms are 180° out of phase, destructive interference occurs, giving rise to grey bands, as shown in Fig. 17. Such bands represent contours of constant density, or isopycnals. In addition, if the flow is isentropic, as it is during the early stages of the transition process when ignition is by means of spark discharge, then the isopycnals also represent isobars. The isopycnals, then, provide means for the determination of the pressure profile ahead of the flame.

The density, ρ , in the flow field is given by the following relationship:

$$\rho(x,y) = \rho_o + CS(x,y) \quad A.1$$

where S is the fringe shift, C is a constant and the subscript o denotes the undisturbed state. The constant C is given by:

$$C = \frac{\lambda}{KL} \quad A.2$$

where λ is the wave length of light, L the physical path length through the test medium, and K the Gladstone-Dale coefficient, which for a given gas is constant and given by the equation:

$$K = \frac{n - 1}{\rho} \quad A.3$$

where n is the index of refraction.

The constants A_1 and B_1 for a $2H_2 + O_2$ mixture were found from an expression of the form:

$$(X_1)_{\text{mix}} = m_{H_2} (X_1)_{H_2} + m_{O_2} (X_1)_{O_2} \quad A.6$$

where m is the mole fraction of the constituent gases. With $m_{H_2} = 0.667$, $m_{O_2} = 0.333$, and using the information given in Table 1A equation A.6 yields:

$$\left. \begin{aligned} A_1 &= 17.92 \times 10^{-5} \\ B_1 &= 6.82 \times 10^{-11} \end{aligned} \right\} \text{ for } 2H_2 + O_2 \text{ mixture}$$

Substituting these values into equation A.5 and using $\lambda = 5.51 \times 10^{-5} \text{ cm}$, the index of refraction for the test mixture was found to be:

$$n_0 = 1.0001835$$

The value of L in equation A.4 is the length of the light path through the test medium which, in this case, is the width of the detonation tube, $L = 3.81 \text{ cm}$.

Substituting the above values of L , λ and n_0 into equation A.4 yields an expression for the density ratio, ρ/ρ_0 , as a function of the fringe shift S :

$$\frac{\rho}{\rho_0} = 1 + .0789 S \quad A.7$$

Since the isopycnals are a manifestation of the condition where the flow fringes are 180° out of phase with the no-flow fringes, S will take on values of $\frac{1}{2}$, $1\frac{1}{2}$, $2\frac{1}{2}$, etc., starting with the first isopycnal.

Finally, when the process can be considered isentropic, the pressure in the flow ahead of the flame can be calculated with sufficient accuracy from the isentropic law with a constant exponent $\gamma = 1.4$.

Table A.2 summarizes the calculations of density and pressure for the composite interferogram shown in Fig. 16.

where d is the fringe spacing, l the fringe displacement measured from its position behind the shock wave, and subscript 1 denotes conditions immediately behind the shock wave. Although the fringes between the flame and shock wave were not straight, they were very nearly parallel. Hence the use of any one of the fringes would yield a sufficiently accurate representation of the average density at a given cross-section. Actually, there was little choice involved, since most of the fringes were displaced out of the field of view. The fringe spacing, d , was measured from the uniform undisturbed field and found to be 1.55 mm.

The index of refraction, n_1 , was calculated using the Gladstone-Dale constant

$$K = \frac{n_1 - 1}{\rho_1} = \frac{n_0 - 1}{\rho_0}$$

with $\rho_0 = 0.03 \text{ lb/ft}^3$, $\rho_1 = 0.0553 \text{ lb/ft}^3$, and $n_0 = 1.000835$, then,

$$\begin{aligned} n_1 - 1 &= \frac{\rho_1}{\rho_0} (n_0 - 1) \\ &= 3.38 \times 10^{-4} \end{aligned}$$

Substituting the values for L , λ , n_1 , and d into equation A.9 yields

$$\frac{P}{P_1} = 1 + 0.275 \lambda \quad \text{A.10}$$

The pressure ratio $\frac{P}{P_1}$ was then computed using the isentropic law, equation A.8.

The rarefaction zone observed immediately ahead of the flame was separated from the preceding compression wave by a sharply defined front. The convex shape of the front indicated that the rarefaction zone did not fill the entire tube cross-section. Hence, a ray of light which passed through the rarefaction also passed through the more highly compressed

TABLE A.2

CALCULATION OF DENSITY AND PRESSURE
IN FLOW AHEAD OF THE FLAME (See Fig. 16)

SUPERPOSITION METHOD

S	x cm	ρ/ρ_0	P/P ₀
0		1.0	1.0
$\frac{1}{2}$	10.8 $\begin{smallmatrix} -.4 \\ +.2 \end{smallmatrix}$	1.04	1.06
$1\frac{1}{2}$	9.6 $\begin{smallmatrix} -.4 \\ +.2 \end{smallmatrix}$	1.12	1.17
$2\frac{1}{2}$	8.5 $\begin{smallmatrix} -.5 \\ +.2 \end{smallmatrix}$	1.20	1.28
$3\frac{1}{2}$	7.4 $\begin{smallmatrix} -.4 \\ +.2 \end{smallmatrix}$	1.28	1.40
$4\frac{1}{2}$	6.3 $\begin{smallmatrix} -.4 \\ +.3 \end{smallmatrix}$	1.36	1.54
$5\frac{1}{2}$	5.3 $\begin{smallmatrix} -.3 \\ +.3 \end{smallmatrix}$	1.43	1.66
$6\frac{1}{2}$	4.5 $\begin{smallmatrix} -.3 \\ +.2 \end{smallmatrix}$	1.51	1.79
$7\frac{1}{2}$	3.6 $\begin{smallmatrix} -.2 \\ +.2 \end{smallmatrix}$	1.59	1.92
$8\frac{1}{2}$	3.0	1.67	2.05

x - distance from the ignitor

TABLE A.3

CALCULATION OF DENSITY AND PRESSURE IN
FLOW AHEAD OF THE FLAME (SEE FIG. 18)

FRINGE DISPLACEMENT METHOD

x cm	l cm	$\frac{P_2}{P_1}$	$\frac{P_2}{P_0}$	$\frac{P_2}{P_1}$	$\frac{P_2}{P_0}$
28.1		1	1.845	1	2.423
28.0	0.25	1.0686	1.97	1.097	2.66
27.5	0.92	1.254	2.32	1.373	3.33
27.0	1.24	1.340	2.47	1.506	3.65
26.5	1.50	1.412	2.61	1.62	3.92
26.0	1.82	1.500	2.77	1.764	4.28
25.5	2.06	1.565	2.89	1.87	4.53
25.0	2.24	1.616	2.98	1.96	4.75
24.9	(1.907)	1.525	2.87	1.805	4.36
24.8	(1.89)	1.520	2.80	1.795	4.34

Note: (l) - corrected fringe displacement.

DISTRIBUTION LIST

AeroChem Research Laboratory
Princeton, New Jersey
ATTN: Dr. H. F. Caloote

Aerojet-General Corp.
San Ramon, California
ATTN: Mr. John Luce

Aeronutronics, Div. of Ford Motor Co.
P.O. Box 697
Newport Beach, Calif.
ATTN: Library

Allison Division
General Motors Corporation
Indianapolis 6, Indiana
ATTN: Mr. T. L. Rosebrook

Armour Research Foundation
10 West 35th St.
Chicago 16, Illinois
ATTN: R. L. Watkins

Arnold Engineering Development Center
ATTN: AEGP
AEO
Arnold Air Force Station, Tenn.

Atlantic Research Corp.
Alexandria, Va.
ATTN: Dr. R. Friedman

AVCO-Everett Research Laboratory
2385 Revere Beach Parkway
Everett 49, Mass.
ATTN: Dr. A. R. Kantrowitz

AVCO-Everett Research Laboratory
2385 Revere Beach Parkway
Everett 49, Mass.
ATTN: Dr. R. Patriok

AVCO-Everett Research Laboratory
2385 Revere Beach Parkway
Everett 49, Mass.
ATTN: Dr. S. Janes

California Institute of Technology
Pasadena, Calif.
ATTN: Mr. Marble

University of California
Berkeley 4, California
ATTN: Professor L. Talbot

Air Force Cambridge Research Center
Geophysics Division
Laurence G. Hanscom Field
Bedford, Mass.
ATTN: Morton A. Levine

Chicago Midway Labs
Chicago, Illinois
ATTN: P. J. Diokerman

University of Chicago
Chicago, Illinois
ATTN: Mr. T. Bonin

Columbia University
New York, New York
ATTN: Dr. Robert Gross

Cornell University
Ithaca, N. Y.
ATTN: Dr. W. R. Sears

Electro-Optical Systems, Inc.
125 N. Vinedo Ave.
Pasadena, Calif.
ATTN: Mr. Webb

General Electric Co.
Evendale, Ohio
ATTN: Dr. M. L. Ghai

General Electric Co.
Philadelphia, Penn.
ATTN: G. W. Sutton

Litton Industries
336 No. Foothill Rd.
Beverly Hills, Calif.
ATTN: Mr. E. L. DeGraeve

University of Maryland
College Park, Maryland
ATTN: Dr. J. M. Burgers

Massachusetts Institute of Technology
Cambridge 39, Mass.
ATTN: Library

University of Minnesota
Minneapolis, Minn.
ATTN: Dr. E. R. Eckert

National Bureau of Standards
Washington 25, D.C.
ATTN: Dr. C. M. Tohen

Northwestern University
Evanston, Illinois
ATTN: Mr. A. B. Cambel

Ohio State University
Columbus, Ohio
ATTN: Library

Pennsylvania State University
University Park, Pa.
ATTN: Dr. H. Li

Princeton University
Princeton, New Jersey
ATTN: Dr. S. M. Bogdonoff

Radio Corporation of America
Princeton, New Jersey
ATTN: Dr. Hutter

Rand Corporation
1700 Main St.
Santa Monica, Calif.

Reaction Motors Division
Thiokol Chemical Corp.
Denville, N. J.
ATTN: Dr. Wolfhard

Republic Aviation Corp.
Conklin St.
Farmingdale, L.I., N.Y.
ATTN: Mr. A. E. Kunen

University of Maryland
College Park, Maryland
ATTN: Mr. H. R. Griem

Rocketdyne
Canoga Park, California
ATTN: Dr. R. Boden

University of Southern California
Los Angeles 7, Calif.
ATTN: Dr. R. L. Chuan

Space Technology Laboratories
P.O. Box 95001
Los Angeles 45, Calif.
ATTN: Dr. David B. Langmuir

Stevens Institute of Technology
Hoboken, N. J.
ATTN: Dr. W. Bostick

Temple University
Philadelphia, Pa.
ATTN: Dr. Lloyd Bohn

Texaco Experiment, Inc.
Richmond 2, Va.
ATTN: Dr. King

Thompson Products, Inc.
23555 Euclid Ave.
Cleveland 17, Ohio
ATTN: Mr. S. H. Fairweather

Professor Osman Mawardi
Case Institute of Technology
Cleveland, Ohio

The Warner & Swasey Co.
Control Instrument Division
34 West 33rd St.
New York, New York
ATTN: Mr. R. H. Tourin

Aeronutronics, Division of Ford Motor Co.
P.O. Box 697
Newport Beach, Calif.
ATTN: Dr. R. Hoglund

Aerojet General Corp.
Azusa, California
ATTN: Dr. Himricks

Plasmadyne Corp.
Santa Ana, Calif.
ATTN: Mr. A. C. Ducati

Plasmadyne Corp.
Santa Ana, Calif.
ATTN: Dr. H. G. Loos

United Aircraft Corp.
East Hartford, Conn.
ATTN: Dr. R. G. Meyerand, Jr.

ASD (ASRMPE)
Wright-Patterson AFB
Dayton, Ohio

ASD (RRLN)
Wright-Patterson AFB
Dayton, Ohio

ASD (ASRC)
Wright-Patterson AFB
Dayton, Ohio

ASD (ASRNE)
Wright-Patterson AFB
Dayton, Ohio

ASD (ASRMD)
Wright-Patterson AFB
Dayton, Ohio